JOURNAL OF AIRCRAFT
Vol. 39, No. 5, September–October 2002

Assessment of Rotor Blade Angle of Attack from Experimental Inflow Data

Susan Althoff Gorton*
NASA Langley Research Center, Hampton, Virginia 23681-2199
and
Danny R. Hoad†
U.S. Army Research Laboratory, Hampton, Virginia 23681-2199

A series of experiments was conducted by NASA Langley Research Center and the U.S. Army, over a 10-year period beginning in the mid-1980s, to provide some insight into the nature of helicopter rotor-system-induced velocity and to provide calibration data for many promising computational methods. Rotor-induced velocities were measured above the rotor system for several forward flight-test conditions in the NASA Langley Research Center 14 by 22 Foot Subsonic Tunnel using a 15%-scale, fully articulated, stiff-in-torsion rotor and in a joint government/industry partnership with Bell Helicopter Textron, Inc., for a larger, aeroelastically scaled, bearingless rotor. A two-component laser velocimeter was used to make these measurements in the facility. The data from these tests have been published previously as NASA quick release reports and conference papers, and they are available electronically. Further analyses of the data to assess the local angle of attack of the rotor blades as a function of azimuth, span, and test condition are documented. The results indicate that assessing inflow using the time average of a rotor revolution does not always capture adequately the local effects of blade passage on the inflow distribution. The inflow distribution should be assessed using the average of the blade azimuth-dependent inflow. At advance ratios less than 0.30, the effects of the individual trailing vortices were evident in the inflow measurements, and they have a significant impact on the local blade flow angle. For higher advance ratios, the blade azimuth-dependent inflow velocities differed very little from the time-averaged inflow characteristics. The analyses demonstrated that dynamic twist is significant for aeroelastically scaled rotors and must be measured or modeled to assess the rotor performance accurately.

Nomenclature

R	=	rotor radius, ft
r	=	local radius of the rotor system, ft
u	=	streamwise component of velocity, ft/s
u_i	=	induced component of velocity parallel to the tip path plane (positive downstream), ft/s
V_{tip}	=	rotor blade tip velocity, ft/s
v	=	vertical component of velocity, ft/s
v_i	=	induced component of velocity perpendicular to the tip path plane (positive up), ft/s
x	=	distance behind blade leading edge, in.
α	=	rotor tip path plane angle, positive nose up, deg
α_l	=	rotor blade section local angle of attack, positive nose up, deg
λ_i	=	induced inflow ratio normal to tip path plane, positive up, v_i/V_{tip}
μ_i	=	induced inflow ratio parallel to tip path plane, positive downstream, u_i/V_{tip}
μ_∞	=	main rotor advance ratio, $U_\infty/\Omega R$
Ψ	=	rotor azimuth measured from downstream position positive counterclockwise as viewed from above, deg

Received 13 June 2001; revision received 19 October 2001; accepted for publication 20 January 2002.

*Aerospace Engineer, Flow Physics and Control Branch, Mail Stop 170. Member AIAA.

†Chief, Load and Dynamics Division, Vehicle Technology Directorate, Mail Stop 266.

Introduction

ONE of the difficulties confronting the helicopter industry is the lack of basic data concerning the flow environment, the blade air loads, and the blade motions that influence the performance, the vibration, and the noise of advanced rotors. To define a rotor for certain performance and noise levels, the designer must be able to calculate with confidence the aerodynamic, dynamic, and acoustic characteristics of the rotor system. Tests have shown[1] that accurately modeling the rotor wake aerodynamics is essential for the accurate prediction of the higher harmonic air loads that influence the blade dynamic response and the control system loads. Studies have demonstrated that acoustic prediction techniques provide good results if accurate blade surface pressures are used as input.[2,3] It is, therefore, clear that the accurate prediction of the rotor wake, the blade surface pressures, and the resulting air loads is a prerequisite to the design of new, quiet, advanced rotors. In Refs. 4 and 5, the dependency of the blade air loads on the velocities induced at the rotor blade by the rotor wake and the velocities during the interaction of the blade with the wake vortices that are embedded in the flowfield are discussed. Many methods have been developed to account for the influence of the rotor wake on blade vibratory air loads and dynamic response,[6–10] and several high-quality experimental data sets have been generated to assist in understanding the interactions between the rotor blade and the rotor wake.[11,12] The results of these studies have confirmed the idea that the rotor is a highly coupled environment where the induced flow to the rotor system is an integral part of the iterative calculation process that must be considered for accurate rotor system aerodynamic, dynamic, and acoustic modeling and prediction.

An essential, fundamental element to any prediction of rotor performance, acoustics, and blade response is calculating the angle of attack at which the blade operates. The angle-of-attack calculations are crucial to the accurate prediction of local airfoil aerodynamic response, which then drives the rotor wake response as well as the rotor dynamic response. Although the geometric angle of the blade

section can be calculated from the rotor operating condition, blade twist, and blade inertial properties, the aerodynamic angle of attack requires the knowledge of the inflow velocity that is self-induced by the lifting rotor and the rotor wake. To predict blade performance, noise, and vibration, an accurate calculation of inflow velocity must be included. Existing comprehensive analyses provide several options to the user for calculating the rotor wake structure that computes the wake's induced effects at the blade for angle-of-attack calculation. The accuracy of these methods are typically judged to be the cause of discrepancies in the codes.

To provide some insight into the nature of induced velocity and to provide calibration data for many promising computational methods, NASA Langley Research Center and the U.S. Army conducted a research program with the intent to measure rotor-induced velocity for several test conditions using a 15%-scale, fully articulated, stiff-in-torsion rotor system at NASA Langley Research Center. In addition, a joint government/industry partnership with Bell Helicopter Textron, Inc., was also initiated to expand the test articles to include the measurement of inflow for a larger, aeroelastically-scaled, bearingless rotor. The research program, which spanned six test entries, was conducted in the NASA Langley Research Center 14 by 22 Foot Subsonic Tunnel. The dedicated two-component laser velocimeter system of the facility was used to make azimuthally dependent velocity measurements above the rotor plane at selected radial locations. Time-dependent blade pressure data also were obtained for one of the test conditions with the bearingless rotor. This paper presents the inflow data and the calculated experimental local blade angle of attack for these two rotors and for several test conditions. This paper also provides a comprehensive reference for all associated papers and reports generated by the government in support of the inflow research program.

Test Equipment, Instrumentation, and Procedures

The research program was conducted through a series of test programs in the NASA Langley Research Center 14 by 22 Foot Subsonic Tunnel using the two-component laser velocimeter (LV) system of the facility and both the Army's 2-Meter Rotor Test Stand (2MRTS) with rigid blades and Bell Helicopter Textron's Powered Force Model (PFM) with aeroelastically scaled blades. Five test conditions were evaluated for the rigid rotor, and four conditions were tested for the aeroelastically scaled rotor.

Facility

The NASA Langley Research Center 14 by 22 Foot Subsonic Tunnel is a closed-circuit, atmospheric wind tunnel designed for the low-speed testing of powered and high-lift configurations.[13] When the tunnel is operated in the open test section configuration, the walls and the ceiling are lifted out of the flow and a solid floor remains under the model. In this configuration, the tunnel can achieve a dynamic pressure of about 91.5 lb/ft^2 or a Reynolds number per foot of approximately 1.8×10^6. This investigation was conducted with the tunnel in the open configuration to enhance optical access to the rotor flowfield.

Model Description

2MRTS and Rotor System and Generic Fuselage

The 2MRTS is a general-purpose rotorcraft model testing system that was mounted on a strut in the forward part of the test section. The system consisted of a 29-hp electric drive motor, an oil-cooled transmission, a rotor system collective and cyclic remote control system, and two six-component strain gauge balances used for measuring forces and moments on the rotor system and the generic fuselage shell (ROBIN). The four-bladed rotor hub used for this investigation was fully articulated with viscous lead-lag dampers and coincident flap and lag hinges. Characteristics of the rotor blades tested on the 2MRTS are listed in Table 1. No attempt was made to dynamically scale the rotor blades; rather, they were very rigid to minimize blade aeroelastic response uncertainties. Additional information regarding the blade characteristics is given in Ref. 14. Figure 1 shows the 2MRTS with the rigid, rectangular planform blades and the ROBIN fuselage shell mounted in the tunnel.

Table 1 Blade and hub properties

Parameter	Rigid rotor with 2MRTS hub	Aeroelastic rotor with bearingless hub
Hub type	Fully articulated	Flexbeam, stacked yoke
Number of blades	4	4
Planform shape	Rectangular	Rectangular
Airfoil section	NACA 0012	ALR airfoil (see Ref. 29)
Hinge offset r/R, in.	2.00, 0.06	Not applicable
Root cutout r/R, in.	8.25, 0.24	9.0, 0.19
Pitch–flap coupling angle, deg	0	51.7
Twist, linear, deg	−8.0	−8.0
Radius, ft	2.88	4.0
Airfoil chord, in.	2.6	3.72
Rotor solidity	0.0977	0.0987
Blade stiffness		
Flapwise, lb-in.^{2}	11,500	Distributed (See ref. 29)
Torsional lb-in.^{2}	25,500	Distributed (See ref. 29)
Flapping inertia, slug/ft^2	0.046	0.2151
Lead-lag damping, in.-lb/deg/s	182.4	182.4

A more detailed description of the 2MRTS and the ROBIN fuselage can be found in Ref. 15, and Reference 16 has corrected coefficients for the ROBIN fuselage shape. Because the ROBIN fuselage was used extensively over the period of this research program, there have been many other reports generated that document the properties of the ROBIN and provide insight for computationally modeling the fuselage shape. More information regarding the ROBIN fuselage, its effect on the induced velocities at the rotor plane, steady and unsteady fuselage pressure data, and computational predictions of flow around the fuselage may be found in Refs. 16–26. Wake data obtained in the presence of the ROBIN fuselage was first presented in Ref. 27 and subsequently revised, corrected for a position offset, and republished as Ref. 28.

PFM

Bell Helicopter Textron's PFM is a general-purpose rotor test stand designed to test Mach-scaled rotors from 4 to 10 ft in diameter. The PFM consists of an input quill assembly, pitch and yaw change mechanisms, a dynamic isolater unit, a five-component, strain gauge rotor balance, and a rotor system collective and cyclic remote control system. Rotor mast torque was measured by a separate strain gauge located below the rotor hub attachment point. The PFM was covered with a nonmetric fairing to minimize test stand aerodynamic interference with the rotor. The cross-sectional shape of the fairing was a NACA 0033 airfoil. The advanced lightweight rotor (ALR) was a four-bladed, bearingless, soft in-plane design with two stacked fiberglass flex-beam yokes and four rotor blades with integral cuffs and elastomeric shear dampers. The characteristics of the ALR rotor hub and blades are given in Table 1. Two of the rotor blades were instrumented with dynamic pressure transducers embedded in the blades. The frequency response of the installed transducers was 40 kHz. The pressure data from the leading-edge transducers at several spanwise locations ($r/R = 0.33$, 0.50, 0.58, 0.69, 0.73, 0.81, 0.87, 0.90, 0.94, and 0.96) will be presented later. Figure 2 shows the PFM with the ALR blades mounted in the tunnel. More detailed information regarding the PFM, the ALR blades, and additional blade pressure data may be found in Refs. 29–33. In Ref. 34, the wake data that were acquired using the PFM and the ALR blades are reported.

LV System and Data Acquisition

The LV system was a two-component system with a 3–21 ft focal length operated in the backscatter mode to minimize alignment difficulties between the transmit and receive optics packages. Most components of the system are described in Refs. 35 and 36; therefore, only a brief description will be given here. The streamwise and

Fig. 1 2MRTS with the two-component LV.

vertical components of velocity are measured by optics located on the side of the tunnel, out of the flow. The traversing mechanisms of the two components are computer-controlled to ensure the sample volumes of the two sets of beams are positioned at a single location. As can be seen in Figs. 1 and 2, the traversing mechanism was located along the side of the tunnel and outside the shear layer of the open jet.

Except for its long focal length and zoom lens assembly, the system was a standard fringe-based LV system utilizing four beams to measure two components of velocity. Polystyrene particles (1.7 μm) suspended in an alcohol and water mixture were used to seed the flow. The velocity data were acquired using either time-domain counters or frequency-domain processors depending on the equipment available for the individual test program. The LV data acquisition system was designed to allow acquisition of rotor azimuth position in addition to the velocity measurements so that an azimuthal history of the velocity could be reconstructed in postprocessing.

The LV data acquisition process consisted of placing the sample volume at the measurement location and acquiring data for a period of 2 min or until 4096 velocity measurements were made in each of the longitudinal and lateral components of velocity. The LV measurements were not made in coincidence, instead the flow was assumed to be periodic with rotor blade passage, and each component was allowed to be measured individually. This process dramatically reduced the time required to obtain the LV data. During this process, as was discussed earlier, conditional sampling techniques were employed to associate each measured velocity component (u and v) with the azimuth position of the number one blade at the time when the measurement was made. At the conclusion of the process, the measurement location was changed, and the acquisition process was repeated.

For each measurement location, the raw data for each component were reviewed, collected into probability density functions (histograms), and further processed to improve the signal-to-noiseratio. The data, velocity vs blade azimuth, were binned into 128 bins (2.8-deg azimuth each) for each component. Statistical characteristics for each bin were calculated, primarily mean and standard deviation. The time-average mean velocity for the location was then calculated from the average of the mean data from each of the azimuth bins. When the mean velocity in each bin was used, and this mean was associated with the bin's rotor azimuth position, it was possible to sort the data by azimuthal position, thereby reconstructing a time history of velocity at each measurement location that represented one average rotor revolution.

Measurement Locations and Test Procedures

In all cases, measurements were made at azimuthal increments of 30 deg from $\Psi = 0$ deg at approximately one chord above the tip path plane. The measurements were made at 15 radial locations

Table 2 Test conditions

Parameter	Rigid rotor					Aeroelastic rotor			
Advance ratio μ_∞	0.15	0.23	0.30	0.35	0.40	0.37	0.37	0.37	0.37
Thrust coefficient C_T	0.0063	0.0064	0.00649	0.0064	0.0064	0.0081	0.0081	0.0064	0.0064
Tip speed V_{tip}, ft/s	624.3	624.5	622.7	624.0	624.0	710.9	605.2	708.9	606.1
Tip Mach number M_{tip}	0.553	0.548	0.536	XX	XX	0.617	0.525	0.618	0.525
Torque coefficient C_Q	0.00036	0.00035	0.00043	0.00048	0.00063	0.00063	0.00061	0.00044	0.00042
Tip path plane angle of attack α, deg	−3.0	−3.0	−4.0	−5.7	−6.8	−5.9	−5.8	−5.8	−5.9
Freestream velocity U_∞, ft/s	94	144	188	219	251	262	223	261	223
Collective A_0, deg	9.4	8.2	10.3	9.2	9.4	14.0	13.2	11.3	10.4
Lateral cyclic A_1, deg	−1.1	−1.5	−1.6	−0.3	−0.5	−0.9	−2.1	−0.6	−1.6
Longitudinal cyclic B_1, deg	3.2	4.1	5.9	6.8	8.2	11.3	10.9	9.1	8.5
Coning a_0, deg	1.5	1.8	2.1	1.8	1.8	2.7	2.7	1.5	1.4
Lag angle, mean, deg	0.95	0.9	0.9	1.3	1.4	1.0	1.0	0.8	0.8
Drag coefficient C_D	0.0002	0.00005	0.0002	0.0000	0.0000	−0.00057	−0.00056	−0.00032	−0.00032

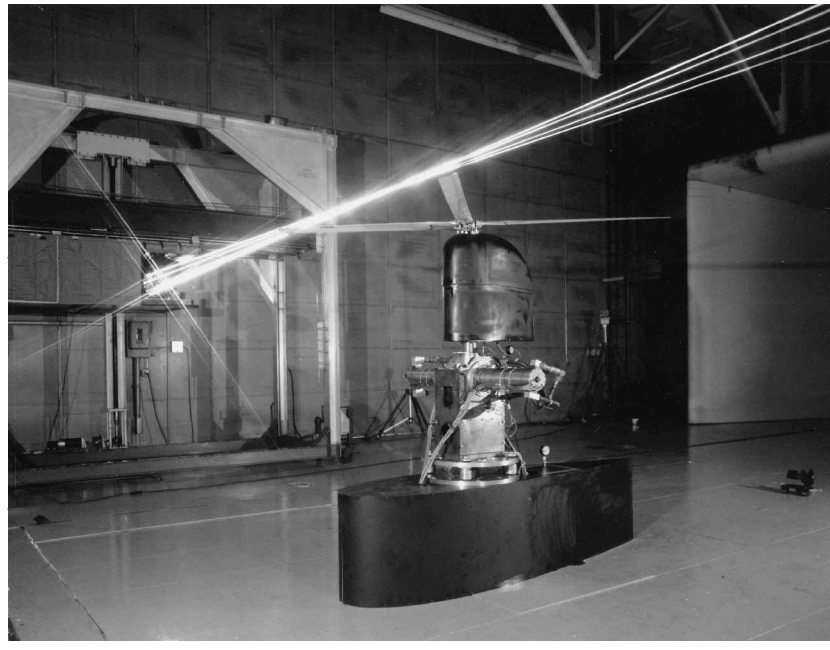

Fig. 2 PFM in the Langley 14 by 22 Foot Subsonic Tunnel with the two-component LV.

concentrated toward the outboard portion of the rotor disk. Table 2 lists the nominal test conditions and selected test parameters for the rigid and the aeroelastic rotor systems. The rotors were trimmed to zero first harmonic blade flapping, and the test condition was held constant over the period of LV data acquisition.

Measurement Uncertainty

Wind-tunnel wall interference corrections were calculated using the methods of Ref. 37 and were considered to be negligible for these configurations at the reported test conditions. The uncertainties associated with the wind-tunnel standard measurements were calculated using the partial derivative analysis method of Ref. 38, and they are documented in Table 3. The uncertainty in the performance data that were measured with the balances is also given in Table 3, as well as the uncertainty in the rotor control angles. The largest contributors to the uncertainty in the LV velocity measurements are the measurement of the crossbeam angles and the particle lag. Using the error estimation techniques described in Refs. 39 and 40, the LV system error for the velocity measurements in this paper is estimated at less than 2.1% of the measured velocity for each component for the rigid rotor and less than 0.92% of the measured velocity for the aeroelastic rotor. The errors in the pressure data attributed to hysteresis, nonlinearity, repeatability, signal conditioning, discriminator circuits, and the analog to digital converter lead to an uncertainty of ± 0.221 lb/in.^{2} Details of the error analysis for each of the LV data sets and the pressure data information may be found in Refs. 29–32 and 41–45.

Blade/Azimuth Dependent Data Analyses

As already discussed, the data exist in two forms: 1) time-averaged velocity components as a function of measurement location and 2) velocity components at a given measurement location as a function of blade 1 azimuth position. It is straightforward to construct the local flow angles to the rotor blades using the time-averaged measurements because it really does not matter where the blade is respective to the measurement location. The process is not so straightforward if the intent is to construct local flow angle to the blade as a function of blade azimuth position. An example of the azimuth dependent data as processed in Refs. 29–32 and 41–45 is presented in Fig. 3. These data represent the time history of the velocity components as the blades pass by the measurement location.

The abscissa on the Fig. 3 plot represents the azimuthal position of blade 1 when the velocity was measured, and of course, the ordinate represents the induced velocity component. In this example, one of the measurement locations was $\Psi = 60$ deg and $r/R = 0.5$, and the component velocities important to calculating the local flow velocity at each of the four blades at the point in time when each blade was at the measurement location are shown as vertical dashed lines on each graph. The velocity components required are those that are not influenced by the local blade circulation, yet are near enough to be represented as the defining flow conditions for airfoil angle-of-attack table-lookup purposes. After some considerable analyses and to be consistent at all measurement locations, the criterion used to select the velocities for the calculation of local flow angle to the blade was when the blade of interest was one chord behind the measurement

Table 3 Measurement uncertainty

Parameter	Uncertainty	
	Rigid rotor	Aeroelastic rotor
Advance ratio	±0.0011	±0.0011
Blade pressures, lb/in.^{2}	Not applicable	±0.221
Collective, deg	±0.5	±0.3
Coning, deg	±0.5	±0.3
Freestream velocity, ft/s	±0.274	±0.274
Lag angle, deg	±0.5	±0.3
Lateral cyclic, deg	±0.5	±0.3
Longitudinal cyclic, deg	±0.5	±0.3
LV velocity measurements, ft/s	<2.1%	<0.92%
Rotor drag, lb	±0.4	±0.5
Rotor lift, lb	±1.0	±1.8
Rotor shaft angle, deg	±0.001	±0.001
Rotor drag coefficient	±0.00002	±0.000009
Rotor thrust coefficient	±0.00037	±0.000042
Rotor tip speed, ft/s	±0.6	±0.8
Rotor tip Mach number	±0.001	±0.001
Rotor torque coefficient	±0.000014	±0.000012

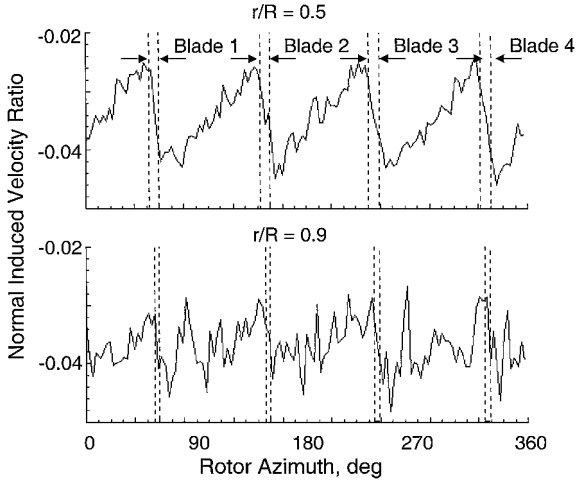

Fig. 3 Example of azimuth-dependent normal induced velocity component for 2MRTS measured at $\Psi = 60$ deg and $r/R = 0.5$ and 0.9.

location. At the tip of the blade, this criterion resulted in using one bin's mean velocity components. At $r/R = 0.2$, this resulted in an average of six measurement bins for all rotor conditions. An example of the difference in this measurement window width is evident by comparing the two window sizes in Fig. 3.

To assure that the selection of the window width did not arbitrarily change the value of the flow angle, the data from two, three, and four chords ahead of each blade were also processed for two complete data sets. The resulting difference in the flow angles computed was very slight. Therefore, all of the data that will be presented in this paper were based on the one chord window. These data were then collected, and distributions of flow angle calculations were made for each blade and an average of the four blades at all nine operating conditions. The velocity components were then used to compute local flow angle to the blade for each blade and an average of all four blades. In addition, these flow angles were computed from the time-averaged results. Only the time-averaged and four-blade-averaged flow angles will be presented. Freestream conditions were included as well as rotor operating conditions: tip path plane angle to the freestream, static twist of the rotor blade, collective, and longitudinal and lateral cyclic as a function of blade azimuth. Dynamic twist was not used in the calculation process. For the 2MRTS data set, this is probably not important because it was stiff in torsion, but it most probably plays a role in the PFM data sets. Unfortunately, there were no dynamic twist data available for the PFM. Therefore, the resulting flow angle calculations at the blade presented in this paper represents the nearest number that can be calculated to obtain the local angle of attack of the airfoil relative to the mean chord line of the airfoil, assuming no dynamic twist due to operating condition.

Discussion of Results

Discussion and theory regarding inflow velocity, its distribution, and effect have been ongoing since the late 1940s (Refs. 6 and 46). Heyson, in Ref. 47, measured inflow using an instrusive probe technique in 1956. To date, the data presented here represent the only nonintrusive measurement of rotor inflow in forward flight. These data also represent the only inflow data that are not time averaged and that were acquired for a bearlingless rotor. The inflow velocity data that were acquired for the rigid and aeroelastic rotors were originally reported in NASA quick release data reports (Refs. 29–34 and 41–45). Portions of the data were also presented as they were acquired (Refs. 33, 35, and 48–51). This paper presents in a summarized, graphical form the inflow data for all of the rigid and aeroelastic rotor test conditions. The inflow data in these publications have been used to calculate local flow angle variation across the rotor disk. As indicated before, the PFM blade set had local surface pressure measurement capability. The only set of pressure data available for the PFM is for one of the four test conditions. These data are available in Ref. 29. A sample of the data is provided in Fig. 4. Shown are the leading-edge pressures near the x/c position of 0.05 for the PFM rotor at $C_T = 0.0064$, $\mu = 0.37$, and $V_{tip} = 711$ ft/s for 10 radial positions along the blade. These inflow and pressure data can also be obtained through a variety of electronic transfer options by contacting the authors.

Inflow

An example of the time-average induced inflow velocities measured above each of the rotor systems at a similar operating condition is shown in Fig. 5. It is obvious from Figs. 5 that the inflow characteristics each rotor experiences at similar operating conditions are similar but different. For both rotors, there is a large area of average upflow over most of the forward part of the rotor disk, and a distinct region of maximum downwash skewed off centerline behind the rotor hub. The PFM rotor has a much greater extent of average upflow and less downwash on the aft part of the disk as compared to the 2MRTS rotor, but the general character of the upwash/downwash is consistent between the two rotors. To determine how these differences affect the flow angle of the rotor system, it was necessary to use the azimuth-dependent data in each data set and process these data as already described.

Flow Angle

The importance of using the azimuth-dependent data to compute flow angle vs using the time-averaged data is shown in Figs. 6–10.

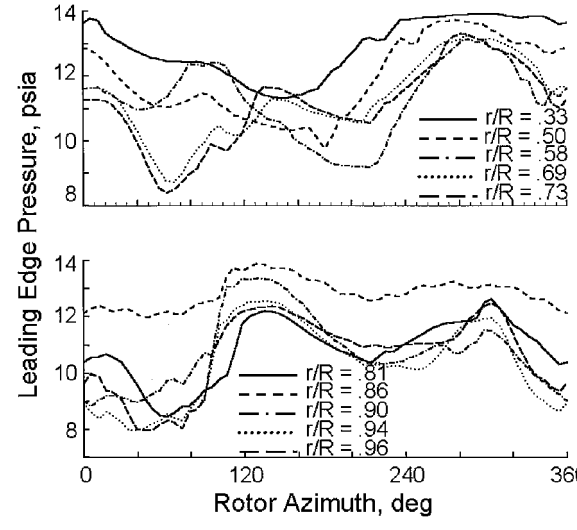

Fig. 4 Example of the leading-edge pressures measured on the PFM rotor at $x/c \sim 0.05$ at $C_T = 0.0064$, $\mu_\infty = 0.37$, and $V_{tip} = 711$ ft/s.

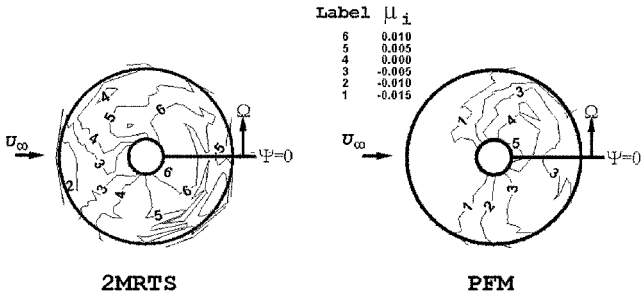

Induced inflow ratio parallel to tip path plane

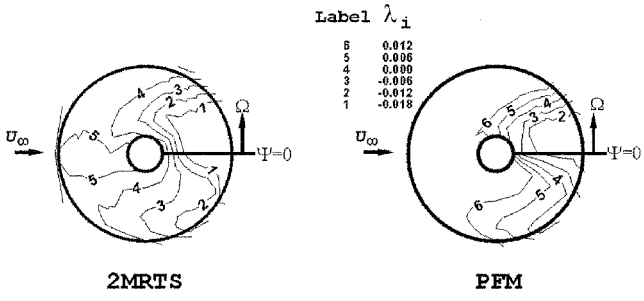

Induced inflow ratio normal to tip path plane

Fig. 5 Time-averaged induced inflow velocity ratios for the 2MRTS and PFM at similar rotor conditions: C_T = 0.0064, $\mu_\infty \sim$ 0.35, and $V_{tip} \sim$ 624 ft/s.

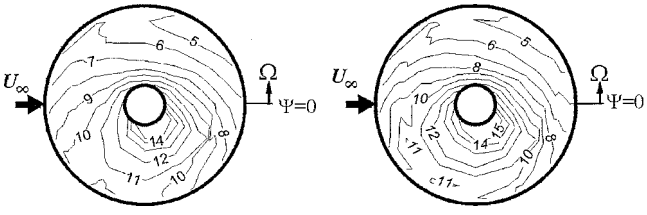

a) Time averaged b) Azimuth dependent

Fig. 6 Flow angle distribution for the 2MRTS at C_T = 0.0064, μ_∞ = 0.15, and V_{tip} = 624 ft/s.

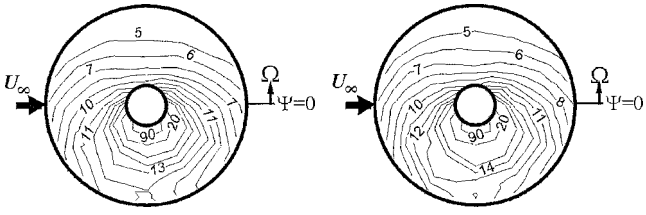

a) Time averaged b) Azimuth dependent

Fig. 7 Flow angle distribution for the 2MRTS at C_T = 0.0064, μ_∞ = 0.23, and V_{tip} = 624 ft/s.

Figures 6–10 present this comparison where the time-average results are provided in Figs. 6a–10a and azimuth-dependent results are provided in Figs. 6b–10b for the five advance ratios tested with the 2MRTS. Because the 2MRTS rotor is very stiff in torsion, the flow angles calculated from the inflow data for this rotor will be a good representation of the angle of attack for the airfoil. From Figs. 6–10, it is evident that the azimuth-dependent calculations are most critical at advance ratios below 0.23. The general shape of the angle-of-attack distribution across the rotor disk is one that can be calculated assuming uniform inflow and is very similar to the classical distributions shown in Refs. 52 and 53. At the lower advance ratios $\mu = 0.15$ and $\mu = 0.23$ (Figs. 6 and 7, respectively), differences between the time-averaged and azimuth-dependent angle of attack can be seen. At higher advance ratios, it appears that the detailed azimuth-dependent inflow measurements are not critical to angle-of-attack calculations. That is, for first-order performance and

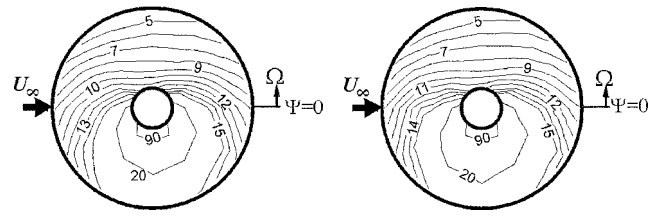

a) Time averaged b) Azimuth dependent

Fig. 8 Flow angle distribution for the 2MRTS at C_T = 0.0065, μ_∞ = 0.30, and V_{tip} = 623 ft/s.

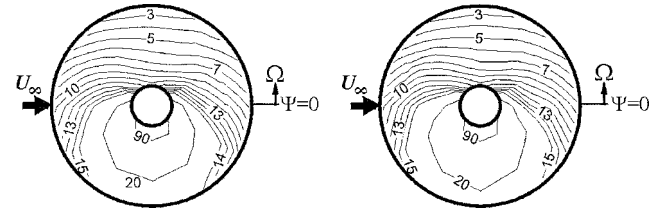

a) Time averaged b) Azimuth dependent

Fig. 9 Flow angle distribution for the 2MRTS at C_T = 0.0064, μ_∞ = 0.35, and V_{tip} = 624 ft/s.

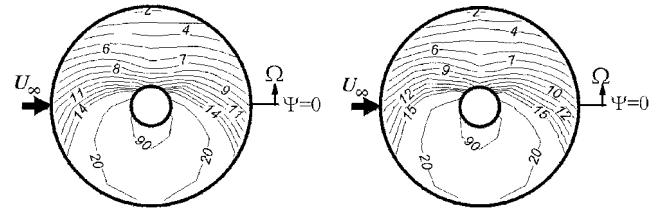

a) Time averaged b) Azimuth dependent

Fig. 10 Flow angle distribution for the 2MRTS at C_T = 0.0064, μ_∞ = 0.40, and V_{tip} = 624 ft/s.

trim calculations at 1-*g* flight conditions simulated in these tests, details of the inflow characteristics at advance ratios above 0.30 are not affected by individual trailing vortex wake effects. This cannot be said for lower advance ratios, or for flight conditions other than 1-*g* level flight trim. Again this is consistent with well-known theory for rotor performance prediction.

As would be expected in trim level flight, the angles of attack to the blade on the advancing side of the rotor disk are small and decrease with increasing advance ratio. Airfoil stall begins to occur on the retreating side above $\mu = 0.23$ on the outboard part of the blade, and this region of potential stall grows with advance ratio. Depending on local conditions (primarily Mach number), the NACA 0012 airfoil will probably maintain attached flow in an unsteady environment to around 16–18 deg, after which the dynamic stall issues become important. Reverse flow is evident on the retreating side where the local angle of attack is greater than 90 deg at advance ratios above 0.23 with increasing areas of extent as the advance ratio is increased.

At $\mu = 0.15$, details of the rotor wake interaction can be seen on both sides of the rotor disk. The contour lines are not as smooth as at higher advance ratios. These effects are indicative of the influence of passage of individual blade tip vortices near each blade. This effect is more pronounced during descending flight but is evident here even in trim, level flight at this low advance ratio. Some of the detailed characteristics of this interaction are lost in the time-averaged results, including a potential region of stall near the root of the blade on the retreating side of the disk. For this advance ratio, there is no evidence of reverse flow over the airfoil, again in keeping with expected results.

The flow angle distributions for the PFM rotor are provided in Figs. 11 and 12. Because this rotor system is aeroelastically scaled, it is not appropriate to refer to the flow angle calculations for these conditions as angle-of-attack measurements. The blades are assuredly

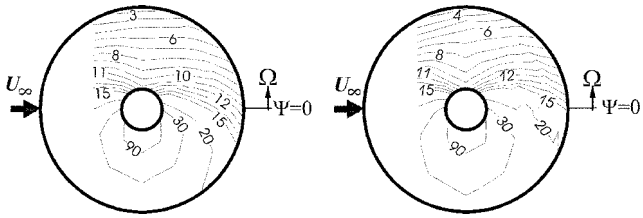

Fig. 11 Flow angle distribution for the PFM at $C_T = 0.0064$ and $\mu_\infty = 0.37$.

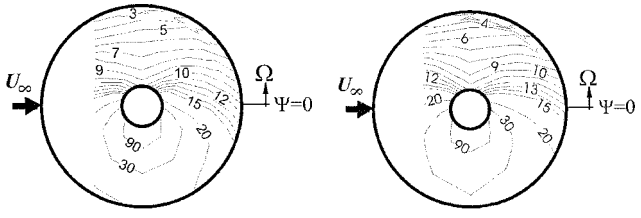

Fig. 12 Flow angle distribution for the PFM at $C_T = 0.0081$ and $\mu_\infty = 0.37$.

experiencing dynamic twist that cannot be accounted for in the calculation process. The azimuth-dependent data from a thrust coefficient of 0.0064 at two different hover tip speeds is presented in Fig. 11 and is repeated for a thrust coefficient of 0.0081 in Fig. 12. The data appear to be truncated on the forward part of the rotor disk. The reason for this is described in detail in the reports in Refs. 29–32. To summarize, the data collected on the front 20% of the rotor disk were at a different operating condition than the back 80%; therefore, it is not appropriate to use it for comparison purposes with the 2MRTS data set. It appears that this rotor system is experiencing a larger area of potential stall, encompassing almost all of the retreating side. This cannot be the case because the rotor system was trimmed at the test condition. Therefore, the only explanation for this is that the blade dynamic twist is not negligible. In fact, the data suggest that the blade dynamic twist on the retreating side was negative and was contributing to counteract the effects of reverse flow. The reverse flow region is evident and is not any different than experienced by the 2MRTS. This is not surprising because the driver for the boundaries of the reverse flow region is the combination of the forward velocity with the rotational velocity at a given radius and is unaffected by dynamic twist. At each thrust coefficient, the size of the apparent stalled region increases with increasing hover tip speed; also note that the PFM aeroelastic rotor data show examples of the local influence of blade vortices passing by the blades, something that was not evident in the torsionally stiff 2MRTS data at these advance ratios.

Fortunately, the PFM and 2MRTS rotor systems were tested at very similar flight conditions: $C_T = 0.0064$, $\mu \sim 0.35$, and $V_{tip} \sim 624$ ft/s. This provides the opportunity to compare two similar rotors, one that is stiff in torsion and the other aeroelastically scaled. This has been done in Fig. 13 as the difference between the normal component of the induced inflow ratio of the PFM and of the 2MRTS and as the difference in resulting flow angle of the PFM with that of the 2MRTS. The induced inflow ratio for the PFM is greater than the 2MRTS all over the disk with the largest values found in pockets on both advancing and retreating side of the rotor disk. A small portion of this increased level of upwash can be attributed to the slightly higher advance ratio as will be explained.

The average momentum induced inflow can be calculated by

$$\bar{\lambda}_i = \frac{-C_T}{2\sqrt{\bar{\lambda}_i^2 + \mu_\infty^2}}$$

For the advance ratio of 0.35, this number is −0.00914, and for the advance ratio of 0.37, this number is −0.00865. The difference

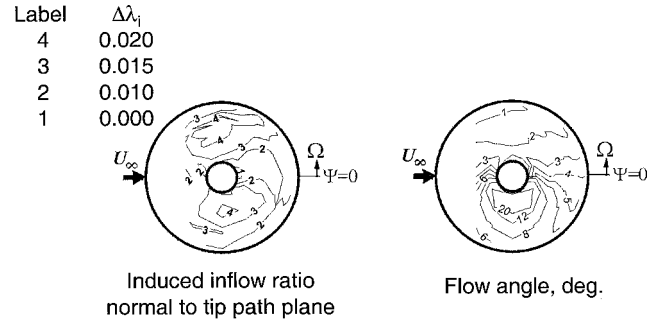

Fig. 13 Difference in inflow characteristics between the PFM and 2MRTS rotor systems at similar operating conditions: $C_T = 0.0064$, $\mu_\infty \sim 0.35$, and $V_{tip} \sim 624$ ft/s.

between these two is 0.0005, far less than the differences experienced between the two data sets. The results of this increase in upwash is to increase the local flow angle to the blade as shown in Fig. 13. These small changes in induced upwash are felt to a greater degree on the retreating side of the blade than on the advancing side because the freestream component of the flow angle calculation is much less on the retreating side of the rotor blade. Differences of 6–20 deg are evident on the retreating side of the blade. This is not possible for the rotor if it is operated in level trimmed flight. Therefore, the dynamic twist of the blade must be a major factor for the performance of these blades. This result emphasizes the need to have some measure of the dynamic twist to assess the angle-of-attack characteristics for aeroelastic rotor systems.

Conclusions

To provide some insight into the nature of induced velocity and to provide calibration data for many promising computational methods, NASA Langley Research Center and the U.S. Army conducted a research program with the intent to measure rotor-induced velocity for several test conditions using a 15%-scale, fully articulated, stiff-in-torsion rotor system at NASA Langley Research Center. In addition, a joint government/industry partnership with Bell Helicopter Textron, Inc., was also initiated to include the measurement of inflow for a larger, aeroelastically scaled, bearingless rotor. The research program, which spanned six test entries, was conducted in the NASA Langley Research Center 14 by 22 Foot Subsonic Tunnel. These data are the only known data for rotor inflow in forward flight that are not time averaged and that document the differences between articulated and bearingless rotor systems. The main conclusions from this program follow.

1) Assessing inflow using the time average of a rotor revolution does not capture adequately the local effects of blade passage on the inflow distribution. The inflow distribution should be assessed using the average of the blade azimuth-dependent inflow.

2) Above advance ratios of 0.30, the rotor inflow closely follows the uniform inflow model and shows little evidence of rotor blade/vortex interaction or influence.

3) At lower advance ratios, the effects of the individual trailing vortices can be seen in the inflow measurements and have a significant impact on the local blade flow angle.

4) The assumption of negligible effects of dynamic twist on the local flow angle appear very reasonable for torsionally stiff blades; however, the effect of dynamic twist is significant for aeroelastically scaled rotors and must be measured or modeled in order to accurately assess the rotor performance.

Acknowledgments

The authors thank the following individuals for their essential contributions to the original research programs: Joe W. Elliott, Richard L. Sailey, W. Derry Mace, John D. Berry, Terence A. Ghee, Judith K. Jumper, Mark S. Chaffin, T. Ben Settle, A. G. Brand, and Martin A. Peryea.

References

[1]Bliss, D. B., Dadone, L., and Wachspres, D. A., "Rotor Wake Modeling for High Speed Applications," *Proceedings of the 43rd Annual Forum of the American Helicopter Society*, St. Louis, MO, 1987, pp. 17–33.

[2]Visintainer, J. A., Burley, C. L., Marcolini, M. A., and Liu, S. R., "Acoustic Predictions Using Measured Pressures From a Model Rotor in the DNW," *Proceedings of the 47th Annual Forum of the American Helicopter Society*, Phoenix, AZ, 1991, pp.791–806.

[3]Ziegenbein, P. R., "The Development of a Prediction Method for the Calculation of Blade–Vortex Interaction Noise Based on Measured Airloads," *The 90's, Decade of Quieter Rotorcraft, An Idea Whose Time is Necessary*, American Helicopter Society and Royal Aeronautical Society, Philadelphia, 1991.

[4]Landgrebe, A. J., and Cheney, M. C., Jr., "Rotor Wakes—Key to Performance Prediction," *Aerodynamics of Rotary Wings*, CP-111, AGARD, 1973.

[5]Gessow, A., "Understanding and Predicting Helicopter Behavior—Then and Now," *Journal of the American Helicopter Society*, Vol. 1, No. 1, 1986, pp. 3–28.

[6]Mangler, K. W., and Squire, H. B., "The Induced Velocity Field of a Rotor," Aeronautical Research Council Reports and Memoranda 2642, London, May 1950.

[7]Ormiston, R. A., "Application of Simplified Inflow Models to Rotorcraft Dynamic Analysis," *Journal of the American Helicopter Society*, Vol. 21, No. 3, 1976, pp. 34–37.

[8]Pitt, D. M., and Peters, D. A., "Rotor Dynamic Inflow Derivatives and Time Constants From Various Inflow Models," *9th European Rotorcraft Forum*, Sept. 1983, pp. 55-2–55-22.

[9]Lal, M. K., Liou, S. G., Pierce, G. A., and Komerath, N. M., "Correlation of Unsteady Pressure and Inflow Velocity Fields of a Pitching Rotor Blade," AIAA Paper 93-3082, July 1993.

[10]Krothapalli, K. R., Prasad, J. V. R., and Peters, D. A., "Study of a Rotor Flap-Inflow Model Including Wake Distortion Terms," *Proceedings of the System Identification for Integrated Aircraft Development and Flight Testing Conference*, Atlanta, GA, March 1999, pp. 1–10.

[11]Lorber, P. F., Stauter, R. C., and Landgrebe, A. J., "A Comprehensive Hover Test of the Airloads and Airflow of an Extensively Instrumented Model Helicopter Rotor," *Proceedings of the 45th Annual Forum*, American Helicopter Society, Boston, MA, 1989, pp. 281–295.

[12]Kube, R., Splettstoesser, W. R., Wagner, W., Seelhorts, U., Yu, Y. H., Tung, C., Beaumier, P., Prieur, J., Rahier, G., and Spiegel, P., "HHC Aeroacoustic Rotor Tests in the German Dutch Wind Tunnel-Improving Physical Understanding and Prediction Codes," *Proceedings of the 52nd Annual Forum of the American Helicopter Society*, Washington, DC, June 1996, pp. 1–16.

[13]Gentry, G. L., Quinto, P. F., Gatlin, G. M., and Applin, Z. T., "The Langley 14- by 22-Foot Subsonic Tunnel: Description, Flow Characteristics, and Guide for Users," NASA TP 3008, Sept. 1990.

[14]Berry, J. D., and May, M. J., "Flapping Inertia for Selected Rotor Blades," NASA TM 104125, Nov. 1991; also U.S. Army Aviation Systems Command AVSCOM TR 91-B-019, Nov. 1991.

[15]Phelps, A. E., and, Berry, J. D., "Description of the Army's 2-Meter Rotor Test System," NASA TM-87762, 1987; also U.S. Army Aviation Systems Command AVSCOM TM-86-B-4, 1987.

[16]Mineck, R. E., "Application of an Unstructured Grid Navier–Stokes Solver to a Generic Helicopter Body," NASA TM-1999-209510, Aug. 1999.

[17]Freeman, C. E., and Mineck, R. E., "Fuselage Surface Pressure Measurements of a Helicopter Wind-Tunnel Model with a 3.15-Meter Diameter Single Rotor," NASA TM 80051, March 1979.

[18]Berry, J. D., and Althoff, S. L., "Computing Induced Velocity Perturbations Due to a Helicopter Fuselage in a Free Stream," NASA TM 4113, June 1989; also U.S. Army Aviation Systems Command, AVSCOM TR 89-B-001, June 1989.

[19]Berry, J. D., and Althoff, S. L., "Inflow Velocity Perturbations Due to Fuselage Effects in the Presence of a Fully Interactive Wake," *46th Annual Forum of the American Helicopter Society*, May 1990, pp. 1111-1120.

[20]Wilson, J. C., "Experimental Evaluation of a Flat Wake Theory for Predicting Rotor Inflow-Wake Velocities," NASA TM 4334, April 1992; also U.S. Army Aviation Systems Command, AVSCOM TR 92-B-004, April 1992.

[21]Berry, J. D., Chaffin, M. S., and Duque, E. P. N., "Helicopter Fuselage Aerodynamic Predictions: Navier–Stokes and Panel Method Solutions and Comparison With Experiment," *American Helicoptor Society Aeromechanics Specialists' Conference*, Jan. 1994, pp. 3.5-1–3.5-20.

[22]Chaffin, M. S., and Berry, J. D., "Navier–Stokes and Potential Theory Solutions for a Helicopter Fuselage and Comparison with Experiment," NASA TM 4566, June 1994; also ATCOM TR 94-A-013, June 1994.

[23]Berry, J. D., "Unsteady Velocity Measurements Taken Behind a Model Helicopter Rotor Hub in Forward Flight," NASA TM 4738, March 1997; also ATCOM TR 97-A-001, March 1997.

[24]Berry, J. D., Letnikov, V., Bavykina, I., and Chaffin, M. S., "A Comparison of Interactional Aerodynamics Methods for a Helicopter in Low Speed Flight," NASA TM-1998-208420, June 1998; also AFDD TR-98-A-003, June 1998.

[25]Boyd, D. D., Jr., Barnwell, R. W., and Gorton, S. A., "A Computational Model for Rotor–Fuselage Interactional Aerodynamics," AIAA Paper 2000-0254, Jan. 2000.

[26]Mineck, R. E., and Gorton, S. A., "Steady and Periodic Pressure Measurements on a Generic Helicopter Fuselage Model in the Presence of a Rotor," NASA TM-2000-210286, June 2000.

[27]Ghee, T. A., and Elliott, J. W., "A Study of the Rotor Wake of a Small-Scale Rotor Model in Forward Flight Using Laser Light Sheet Flow Visualization with Comparisons to Analytical Methods," *48th Annual Forum of the American Helicopter Society*, June 1992, pp. 697–719.

[28]Ghee, T. A., Berry, J. D., Zori, L. A. J., and Elliott, J. W., "Wake Geometry Measurements and Analytical Calculations on a Small-Scale Rotor Model," NASA TP 3584, Aug. 1996; also ATCOM TR-96-A-007, Aug. 1996.

[29]Elliott, J. W., Peryea, M. A., and Brand, A. G., "Induced Inflow Velocity and Blade Surface Pressure Measurements for a Helicopter Model in Forward Flight. Volume 1: Advance Ratio of 0.37, Thrust Coefficient of 0.0081 and Hover Tip Speed of 710 Ft/Sec," NASA TM 104224, April 1992; also U.S. Army Aviation Systems Command, AVSCOM TR-92-B-003, April 1992.

[30]Mace, W. D., Elliott, J. W., Peryea, M. A., Brand, A. G., and Wood, T. L., "Investigation of the Aerodynamic Environment for an Advanced Lightweight Rotor in Forward Flight. Volume 1: Laser Velocimeter Inflow Data, Advance Ratio of 0.37, Thrust Coefficient of 0.0081 and Hover Tip Speed of 603 Ft/Sec," Vol. 1, NASA TM 109040, Nov. 1993; also Vol. 1 ATCOM TR-93-A-012, Nov. 1993.

[31]Mace, W. D., Elliott, J. W., Peryea, M. A., Brand, A. G., and Wood, T. L., "Investigation of the Aerodynamic Environment for an Advanced Lightweight Rotor in Forward Flight. Volume 2: Laser Velocimeter Inflow Data, Advance Ratio of 0.37, Thrust Coefficient of 0.0064 and Hover Tip Speed of 710 Ft/Sec," Vol. 2, NASA TM 109040, Nov. 1993; also Vol. 2, ATCOM TR-93-A-012, Nov. 1993.

[32]Mace, W. D., Elliott, J. W., Peryea, M. A., Brand, A. G., and Wood, T. L., "Investigation of the Aerodynamic Environment for an Advanced Lightweight Rotor in Forward Flight. Volume 3: Laser Velocimeter Inflow Data, Advance Ratio of 0.37, Thrust Coefficient of 0.0064 and Hover Tip Speed of 603 Ft/Sec," Vol. 3, NASA TM 109040, Nov. 1993; also Vol. 3, ATCOM TR-93-A-012, Nov. 1993, p. 14.

[33]Wood, T. L., Brand, A. G., and Elliott, J. W., "An Experimental Investigation of Rotor Blade Airloads and Wake Structure at High Advance Ratio," *46th Annual Forum of the American Helicopter Society*, May 1990.

[34]Mace, W. D., Elliott, J. W., Peryea, M. A., Brand, A. G., and Wood, T. L., "Investigation of the Aerodynamic Environment for an Advanced Lightweight Rotor in Forward Flight. Volume 4: Laser Velocimeter Wake Data, Advance Ratio of 0.37," Vol. 4, NASA TM 109040, Nov. 1993; also Vol. 4, ATCOM TR-93-A-012, Nov. 1993.

[35]Elliott, J. W., Althoff, S. L., Sellers, W. L., III, and Nichols, C., "Inflow Velocity Measurements Made on a Helicopter Rotor Using a Two-Component Laser Velocimeter," AIAA Paper 87-1321, June 1987.

[36]Gorton, S. A., Poling, D. R., and Dadone, L., "Investigation of Blade–Vortex Interaction Using Laser Velocimetry and Pressure-Instrumented Rotor Blades. Volume 1—Advance Ratio of 0.2, Rotor Lift Coefficient Normalized by Solidity of 0.07, and Shaft Angle of 0 Degrees," NASA TM 4570, 1995; also ATCOM-TR-94-A-003, 1995.

[37]Heyson, H. H., "Use of Superposition in Digital Computers to Obtain Wind-Tunnel Interference Factors for Arbitrary Configurations, with Particular Reference to V/STOL Models," NASA TR R-302, 1969.

[38]*Instruments and Apparatus. Part I – Measurement Uncertainty*, American National Standards Inst./American Association of Mechanical Engineers PTC 19.1-1985, American National Standards Inst., New York 1985, pp. 3–33.

[39]Young, W. H., Jr., Meyers, J. F., and Hepner, T. E., "Laser Velocimeter Systems Analysis Applied to a Flow Survey Above a Stalled Wing," NASA TN D-8408, Aug. 1977.

[40]Dring, R. P., "Sizing Criteria for Laser Anemometry Particles," *Journal of Fluids Engineering*, Vol. 104, March 1982, pp. 15–17.

[41]Elliott, J. W., Althoff, S. L., and Sailey, R. H., "Inflow Measurements Made with a Laser Velocimeter on a Helicopter Model in Forward Flight, Volume I: Rectangular Planform at an Advance Ratio of 0.15," NASA TM 100541, April 1998; also U.S. Army Aviation Systems Command AVSCOM TM 88-B-004, April 1988.

[42]Elliott, J. W., Althoff, S. L., and Sailey, R. H., "Inflow Measurements Made with a Laser Velocimeter on a Helicopter Model in Forward Flight, Volume II: Rectangular Planform at an Advance Ratio of 0.23," NASA TM 100542 April 1998; also U.S. Army Aviation Systems Command AVSCOM TM 88-B-005, April 1988.

[43]Elliott, J. W., Althoff, S. L., and Sailey, R. H., "Inflow Measurements Made with a Laser Velocimeter on a Helicopter Model in Forward Flight, Volume III: Rectangular Planform at an Advance Ratio of 0.30," NASA TM 100543, April 1998; also U.S. Army Aviation Systems Command AVSCOM TM 88-B-006, April 1988.

[44]Hoad, D. R., Althoff, S. L., Elliott, J. W., and Sailey, R. H., "Inflow Measurements Made With a Laser Velocimeter on a Helicopter Model in Forward Flight—Volume VI: Rectangular Planform Blades at an Advance Ratio of 0.35," NASA TM 101598, April 1989; also U.S. Army Aviation Systems Command AVSCOM TM 89-B-001, April 1989.

[45]Hoad, D. R., Althoff, S. L., Elliott, J. W., and Sailey, R. H., "Inflow Measurements Made with a Laser Velocimeter on a Helicopter Model in Forward Flight-Volume VII: Rectangular Planform Blades at an Advance Ratio of 0.40," NASA TM 101599, April 1989; also U.S. Army Aviation Systems Command AVSCOM TM 89-B-002, April 1989.

[46]Berry, J. D., Hoad, D. R., Elliott, J. W., and Althoff, S. L., "Helicopter Rotor Induced Velocities—Theory and Experiment," *American Helicopter Society Specialists' Meeting on Aerodynamics and Aeroacoustics*, Feb. 1987, p. 10.

[47]Hoad, D. R., Althoff, S. L., and Elliott, J. W., "Rotor Inflow Variability with Advance Ratio," *44th Annual Forum of the American Helicopter Society*, June 1988, pp. 57–72.

[48]Althoff, S. L., "Effect of Tip Speed on Rotor Inflow," *Journal of the American Helicopter Society*, Vol. 34, No. 4, 1989, pp. 18–27.

[49]Hoad, D. R., "Rotor Induced-Inflow-Ratio Measurements and CAMRAD Calculations," NASA TP 2946, Jan. 1990; also U.S. Army Aviation Systems Command AVSCOM TM 89-B-010, Jan. 1990.

[50]Dress, I. J. M., "A Theory of Airflow Through Rotors and its Application to Some Helicopter Problems," *Journal of the Helicopter Society of Great Britain*, Vol. 3, No. 2, 1949, pp. 79–104.

[51]Heyson, H. H., "Analysis and Comparison with Theory of Flowfield Measurements Near a Lifting Rotor in the Langley Full-Scale Tunnel," NACA TN-3691, April 1956.

[52]Johnson, W., "Forward Flight II," *Helicopter Theory*, Princeton Univ. Press, Princeton, NJ, 1980, pp. 198–201.

[53]Gessow, A., and Meyers, G. C., Jr., "The Prediction and Effects of Rotor Blade Stall," *Aerodynamics of the Helicopter*, 8th ed., College Park Press, College Park, MD, 1985, pp. 251–253.